NASA TECHNICAL NOTE

NASA TN D-5326

NASA TN D-5326

CORROSION IN A COBALT ALLOY, TWO-PHASE MERCURY LOOP

by Alex Vary, Coulson M. Scheuermann, Louis Rosenblum, and Warren H. Lowdermilk

Lewis Research Center
Cleveland, Ohio

NATIONAL AERONAUTICS AND SPACE ADMINISTRATION • WASHINGTON, D. C. • JULY 1969

NASA TN D-5326

CORROSION IN A COBALT ALLOY, TWO-PHASE MERCURY LOOP

By Alex Vary, Coulson M. Scheuermann, Louis Rosenblum,
and Warren H. Lowdermilk

Lewis Research Center
Cleveland, Ohio

NATIONAL AERONAUTICS AND SPACE ADMINISTRATION

For sale by the Clearinghouse for Federal Scientific and Technical Information
Springfield, Virginia 22151 – CFSTI price $3.00

ABSTRACT

A two-phase mercury corrosion loop was operated for 1147 hr at a peak liquid temperature of 1075° F (858 K). The loop was constructed of the cobalt-base alloy HS-25 (L-605). The maximum corrosion occurred in the boiler inlet near the point where two-phase flow began and the liquid temperature peaked. The loop results were compared with corrosion capsule tests and other loops of the same alloy. The corrosion markedly exceeded that found in either the reflux capsules or low-flow-velocity loops operated at the same temperature.

CORROSION IN A COBALT ALLOY, TWO-PHASE MERCURY LOOP

by Alex Vary, Coulson M. Scheuermann, Louis Rosenblum, and Warren H. Lowdermilk

Lewis Research Center

SUMMARY

A two-phase, forced-convection loop was used to study corrosion in a mercury boiler. The loop was a monometallic, tubular flow circuit constructed of the cobalt-base alloy HS-25 (L-605). In the boiler, the peak liquid temperature was 1075° F (858 K), and in the superheater, the vapor temperature was 1300° F (977 K). The loop was operated for a total of 1147 hours with a liquid velocity of about 8 feet per second (240 cm/sec) at the boiler inlet.

A maximum penetration depth of 10 mils (2.5×10^{-2} cm) occurred near the boiler inlet where two-phase flow began and the liquid temperature reached its peak value. In this region, the potential for dissolutive attack was the greatest because of the exponential increase of the solubility of the alloy elements with temperature. The attack was by selective solution (leaching) of mercury-soluble elements. The leached layer was a residue composed chiefly of the relatively insoluble compounds, Co_3W and carbides of the M_6C-type structure.

The loop data were compared with data obtained with mercury reflux capsules and other loops of the same alloy operated at approximately the same temperature in the zone of maximum attack. In this loop, the maximum penetration markedly exceeded that found in either the reflux capsules or low-flow-velocity loops. This result was ascribed to the effect of liquid flow velocity on the corrosion rate during a critical initial stage of the corrosion process. Further comparison with HS-25 reflux capsule data led to inferences concerning the corrosion mechanisms in the loop. In addition to the corrosion processes in the region of maximum attack, other complex mass transfer phenomena found in the loop are discussed.

A prominent role in the analysis of the loop results was played by an X-ray image system by means of which pertinent aspects of the mercury flow pattern were determined.

INTRODUCTION

Mercury is one of the working fluids applicable to nuclear-powered Rankine cycle turboelectric systems for space use. In the SNAP-8 system, for example, mercury vapor drives a turbogenerator to produce from 30 to 100 kilowatts of electric power (ref. 1). Because of this potential use of mercury, studies have been directed toward understanding mercury corrosion processes (refs. 2 to 4). A recent series of reflux capsule experiments (ref. 4) revealed the existence of significant changes in the rate-controlling processes that occur during mercury corrosion. A number of low-velocity, two-phase loop experiments revealed corrosion effects and deposit accumulations that have adverse effects on loop performance (refs. 5 to 7). In addition, previous work demonstrates the effect of liquid velocity on corrosion rates in forced-flow loops (see refs. 8 and 9).

The purpose of the loop experiment described herein was to contribute to the understanding of corrosion processes that are likely to arise in a two-phase forced-flow mercury boiler. Close attention was focused on the effect of high liquid velocity on the corrosion rate. The material for this loop study, the cobalt-base alloy HS-25 (L-605), was selected because the results could be readily compared with previous data from refluxing capsules such as that reported in reference 4.

The corrosion loop described herein produced long periods of stable performance. Consequently, many of the problems that might have hindered the interpretation of results, such as boiling instabilities, frequent flow fluctuations, and copious liquid entrainment effects, did not occur. The loop was operated for 1147 hours at a peak liquid temperature of approximately 1075° F (858 K) and at an average liquid velocity of 8 feet per second (240 cm/sec). The significant features of loop design and performance and the results of post-test examination are described herein.

APPARATUS

General Description of Loop

The mercury loop consisted of the following major components: preheater, boiler, superheater, vapor throttle, condenser, condensate column, electrodynamic mercury pump, and flowmeter, as shown in figures 1 to 3. The material of construction was HS-25 (L-605), a cobalt-base alloy. For most of the loop, the material was used in the fully annealed condition; however, in the boiler-superheater, the material was cold worked by a swaging process used to fabricate a helical groove. The weight percent composition of a typical sample of HS-25 was cobalt, 52; chromium, 19.5; tungsten, 14.4; nickel, 9.75; manganese, 1.45; iron, 1.34; silicon, 0.52; carbon, 0.10; phosphorus, 0.0003; and sulfur, 0.0003.

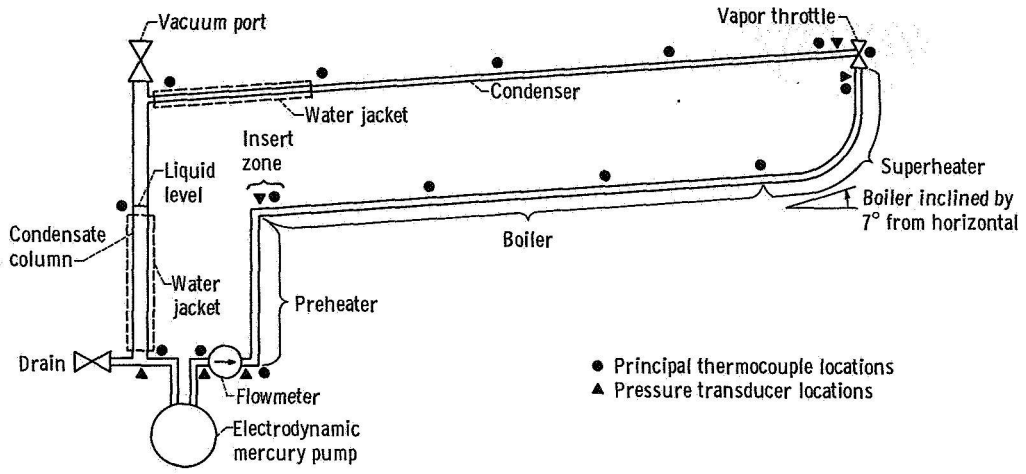

Figure 1. - Two-phase mercury corrosion loop.

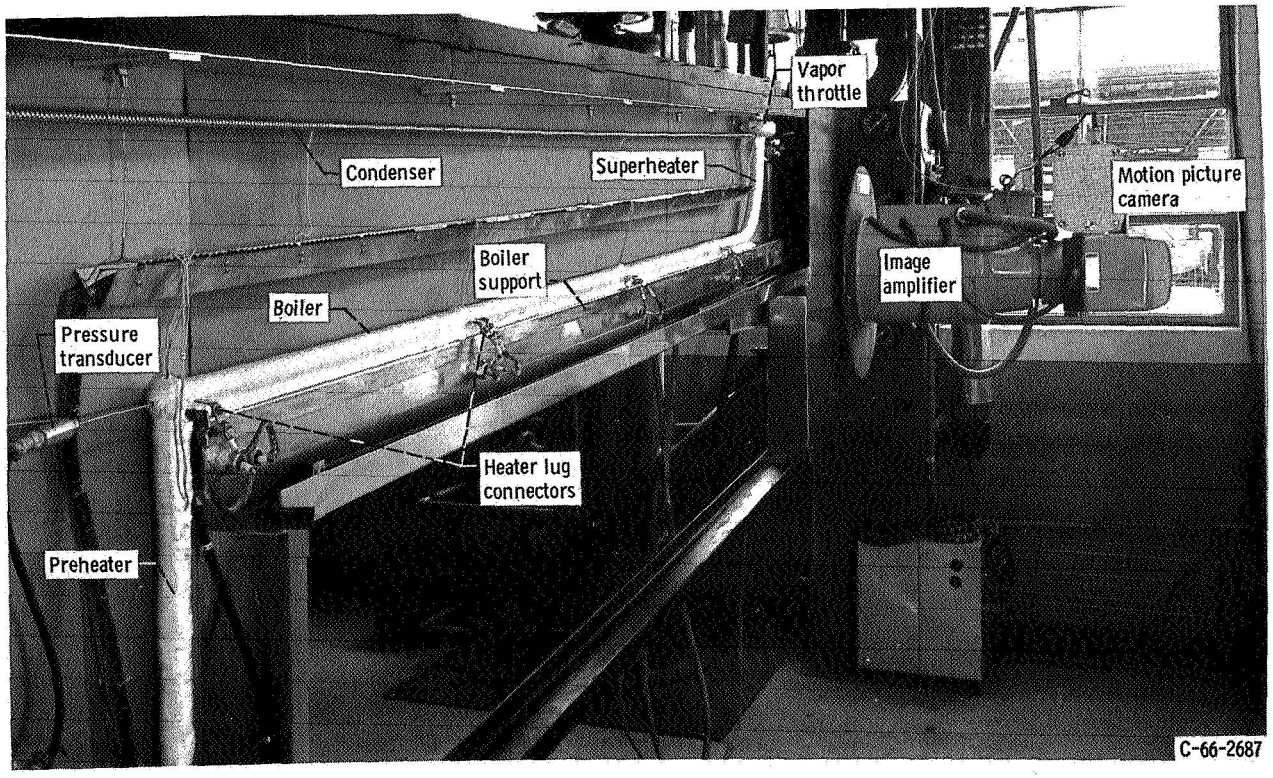

Figure 2. - Front view of mercury corrosion loop.

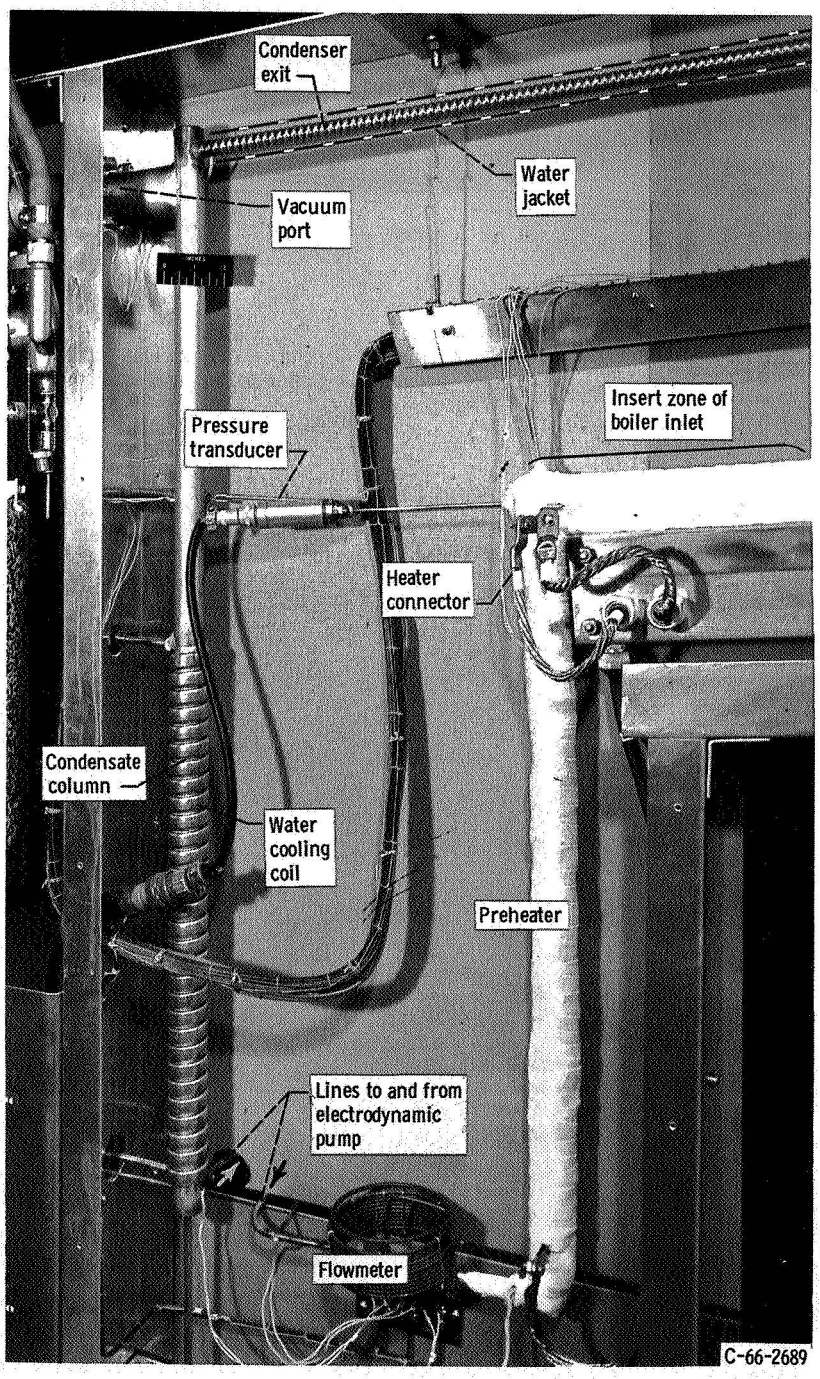

Figure 3. - Condensate end of mercury loop (condenser exit water-cooling jacket was added as outlined).

After fabrication and vacuum pumpdown, the loop was charged with triple-distilled mercury. The mercury was heated by electrical heater elements (fig. 4) surrounding the preheater, boiler, and superheater. The condenser was cooled by radiation and natural (air) convection. At the exit end of the condenser, a water-jacketed channel subcooled the liquid mercury before it reentered the pump and preheater.

The physical arrangement and design of the loop components were tailored to permit the use of an X-ray photographic image system for viewing boiling and condensing flow patterns (see fig. 2). An X-ray traverse apparatus permitted scanning and examination of any part of the loop from the boiler inlet through the condenser exit. At regular intervals, fluorographic motion-picture records were made of boiler-superheater and condenser scans for future study.

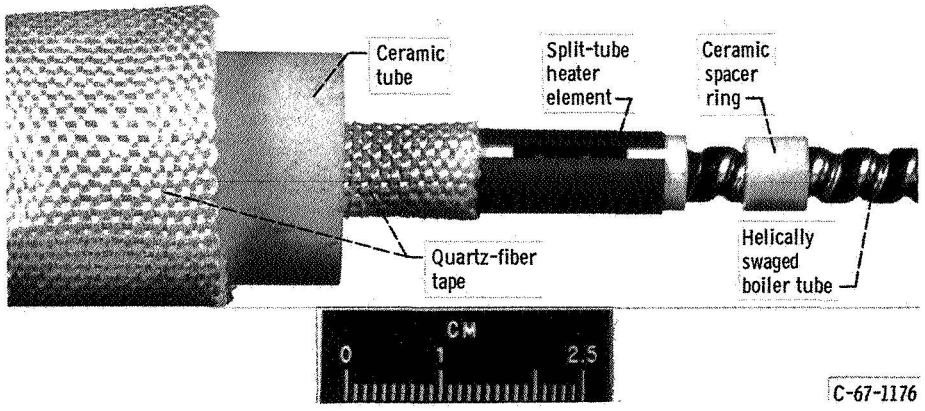

Figure 4. - Cutaway mockup of insulation and electric heater element used to heat loop boiler-superheater.

Boiler-Superheater Details

The boiler-superheater consisted of thin-walled tubing having a swaged helical groove along its entire length. The material was cold worked during the swaging process and was not subsequently heat treated. A typical boiler-superheater section is shown in figure 5. The pitch of the helical groove was 1/8 inch (0.32 cm), and the inside diameter of the groove was slightly greater than 1/8 inch (0.32 cm). One continuous length of helically swaged 0.25-inch- (0.64-cm-) outside diameter by 0.020-inch- (0.051-cm-) wall tube comprised the boiler-superheater. The boiler was a straight 90-inch- (228-cm-) long section inclined by about 7^{o} with the horizontal from inlet to outlet as indicated in figure 1 (p. 3). The superheater was a curved 25-inch- (64-cm-) long section with a radius of about 9 inches (23 cm) beginning at the boiler outlet (see figs. 1 and 2).

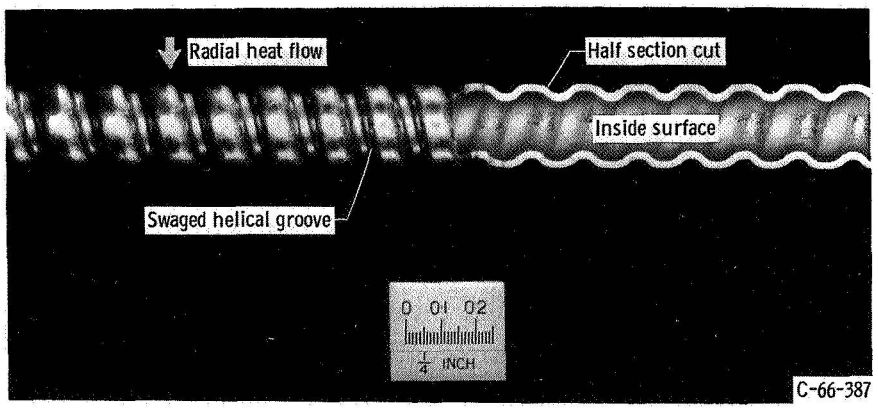

Figure 5. - Typical section of helically swaged tube used in mercury loop boiler and superheater.

The swaged helical groove in the boiler-superheater was provided to help separate the liquid mercury from the mercury vapor phase. This method of phase separation was particularly suited to X-ray scanning.

The inlet end of the boiler contained a 6-inch- (15-cm-) long, 0.125-inch- (0.318-cm-) diameter cylindrical insert. The insert fit tightly inside the swaged boiler tube, and the resultant flow channel was a helical passage around the insert. The purpose of the insert was to reduce the flow cross section and thereby increase the liquid velocity in the boiler inlet. This device helped improve boiler performance by enhancing phase separation by centrifugal action of the liquid in the nucleation zone.

Surface contaminants in the boiler-superheater could inhibit mercury wetting and thereby impair performance. A chemical cleaning procedure was therefore followed to remove contaminants from all loop components (appendix A).

Instrumentation

Thermocouples were spot welded to the surface of the loop tubing. Along the boiler-superheater the thermocouples were attached to the tube in the essentially adiabatic space between heaters and covered with quartz fiber insulation. The locations of the principal thermocouples are identified in figure 1. Additional thermocouples were included for heater power control and automatic shutdown in case of excessive temperature excursions. All significant temperature measurements were made by means of platinum - platinum-13-percent-rhodium thermocouples.

Pressure measurements were obtained with unbonded, strain-gage-type pressure transducers. The transducers were connected to the loop with 0.125-inch- (0.318-cm-) outside diameter, small-bore HS-25 tube. The pressure transmission tubes were welded

to the loop at the locations indicated in figure 1. The previously mentioned insert in the boiler inlet was actually an extension of a pressure transmission tube used to measure pressure in the boiler near the inlet.

The flowmeter consisted of 12 feet (3.7 m) of tubing of 0.125-inch (0.318-cm) outside diameter by 0.0625-inch (0.159-cm) inside diameter. The flow rate was determined by the pressure difference between the flowmeter inlet and exit. The relation between the pressure loss in the flowmeter tube and the flow rate was obtained by direct calibration.

OPERATION AND PERFORMANCE

Principal temperature and pressure conditions in the loop were set to correspond as closely as possible to those contemplated for the SNAP-8 system boiler-superheater (ref. 1). The flow rate and liquid velocities in the loop were chosen to satisfy experimental requirements.

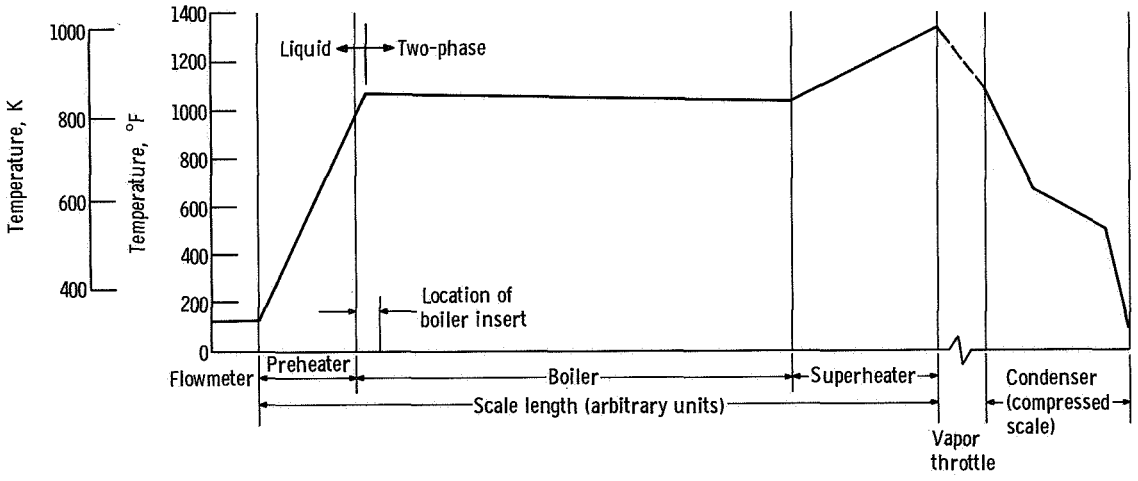

Figure 6. - Temperature profile in mercury loop.

Interest was centered on the boiler inlet where the greatest corrosive attack was anticipated. Care was taken to ensure that the saturation temperature at the location of the boiling interface remained essentially constant throughout the run.

The temperature profile of the loop is shown in figure 6. The variations of the boiler inlet temperature, pressure, and flow rate with test time are plotted in figure 7.

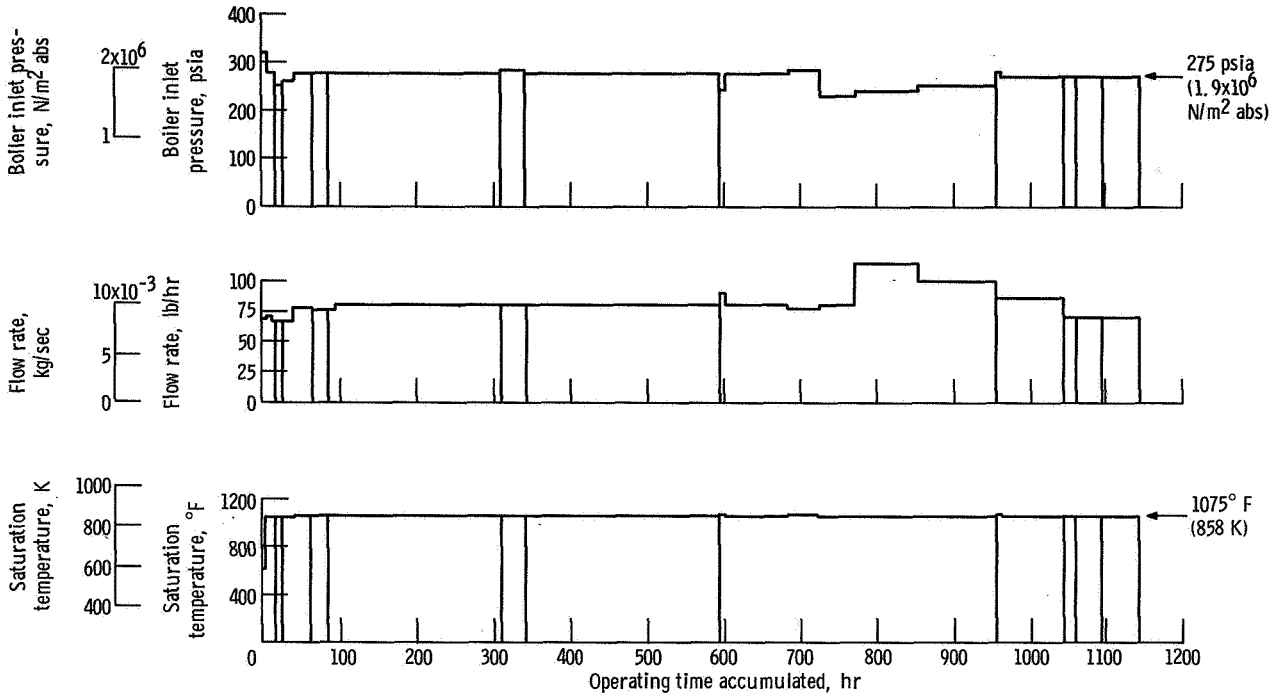

Figure 7. - Pressure, flow rate, and saturation temperature histories of mercury corrosion run. Vertical lines indicate shutdown-startup breaks in run continuity.

Two-Phase Flow Conditions

The average mercury flow rate was 84 pounds per hour (0.0105 kg/sec). Corresponding to this flow rate was a liquid velocity of about 3 feet per second (90 cm/sec) in the liquid-filled helical channel around the insert in the boiler inlet zone. This velocity was calculated with the assumption that no axial leakage flow existed in the insert zone. This assumption was reasonable because of the tight fit between the insert cylinder and the swaged boiler tube. The latter (downstream) half of the insert helix contained simultaneous liquid and vapor flow. Accordingly, the liquid velocity changed with the inception of concurrent liquid-vapor flow. Near the end of the insert, the average liquid velocity during the run was approximately 8 feet per second (240 cm/sec). This velocity is an estimate based on a slip ratio of 3 and a vapor quality of 0.033 at the insert end. The slip ratio and quality correspond closely to the observed void fraction of approximately 0.5. (The quality quoted was based on actual heat-balance measurements.) During about the first 40 hours of the run, the velocity in the insert zone was about 6 feet per second (180 cm/sec). This velocity is significant in view of the velocity effect discussion given in the section Corrosion mechanisms.

Past the end of the insert, X-ray observation showed that the liquid stream persisted in following the helical path along the groove. For this phenomenon to occur, the helical

streamlet should have a tangential velocity of approximately 3.2 feet per second (98 cm/sec). This velocity is not necessarily a minimum because surface energy forces due to wetting supplement the centrifugal forces due to the velocity.

The inception of nucleation and two-phase flow occurred in the insert zone at a point approximately 3 inches (7.5 cm) from the boiler inlet. In this region, the saturation temperature was approximately 1075° F (858 K), and the saturation pressure was approximately 275 psia (1.9×10^6 N/m^2 abs). Although the two-phase inception point had a fairly precise location, it tended to shift position from time to time. In general, the inception point resided near the center of the insert zone. The peak temperature of 1075° F (858 K) previously quoted did not rise or fall by more than 1 percent during the run with the exception of the down times indicated in figure 7.

Within the superheater, the vapor temperature rose from about 1040° F (833 K) at the inlet to about 1350° F (1003 K) at the exit. The superheater exit pressure was approximately 240 psia (1.65×10^6 N/m^2 abs). At the condenser inlet, the temperature was 1100° F (868 K) and the pressure was approximately 10 psia (6.9×10^4 N/m^2 abs). From the condenser exit to the pump inlet, the temperature of the mercury was 80° F (301 K). The condenser exit (vacuum) pressure was between 10 and 100 torr. This pressure was attributed to noncondensable gases that accumulated in the loop. Periodically, a vacuum port over the condensate column was opened to draw off these noncondensables.

Two-Phase Flow Patterns Observed by X-Ray

The helical flow that began in the all-liquid portion of the insert zone of the boiler inlet persisted in the two-phase portion of the insert channel. At the end of the insert zone, the liquid remained separated from the vapor phase. A well-defined helical streamlet of liquid mercury formed in the inside helical grooves of the boiler. Because the X-rays revealed only the bulk liquid flow, the presence of a liquid mercury film covering the boiler wall could be inferred only from other evidence (e.g., from the corrosion-deposition results).

The X-ray scan of the boiler showed that, from the inception of two-phase flow to the end of the boiler, the liquid phase was essentially confined to a helical streamlet that followed the swaged groove. This helical streamlet represented the bulk liquid flow that became shallower as it progressed through the boiler. Near the boiler exit, the streamlet became thinner and its bounds were more diffuse.

Beyond the halfway point of the boiler, the liquid streamlet was rather evenly spread in the helical groove. However, the liquid still flowed in a helical path. Near the boiler exit, the liquid phase consisted of a thin film. Close observation of slight variations in the thickness of this film flow indicated that the liquid phase vanished near the superheater inlet.

Downstream of the superheater inlet, no visual evidence of a liquid phase existed. However, this lack of evidence should not be construed as indicating that no liquid phase whatever passed through the superheater under normal operating conditions. Because of the limitations of the X-ray system, high-quality saturated vapor was indistinguishable from dry, superheated vapor. Likewise, a fine dispersion of liquid entrained in the vapor would have escaped detection.

Off-Design Conditions

During about 10 percent of the 1147-hour run, there were intervals when the conditions in the loop deviated from the normal steady conditions described in the section Two-Phase Flow Conditions. These deviations consisted of cyclic variations of flow, pressure, and temperature triggered by various factors. In addition, 12 shutdowns were occasioned by the need for minor repairs or because of instrument malfunctions (see fig. 7). These shutdown and startup times were brief (less than 15 min) and, hence, were not counted as off-design intervals.

Usually the off-design amplitudes of flow, pressure, and temperature variations were small (less than 10 percent variation in pressure, 2 percent in temperature). The normal conditions constituted the mean about which the deviations ranged. However, toward the last 300 hours of the run, during approximately 1 percent of the 1147-hour run time, occasional abrupt drops in the degree of superheat occurred. During these degraded intervals, not only low-quality (wet) vapor but also liquid streamlets traversed the entire length of the superheater. These off-design conditions are mentioned because they may have produced some of the mass transfer effects described in the ensuing paragraphs.

RESULTS AND DISCUSSION

The mercury loop was operated under two-phase conditions for 1147 hours at a peak liquid temperature of about 1075° F (585 K). The run was terminated as a result of flow channel constriction by deposits in the vapor throttle. After the test, 3/4-inch-(1.9-cm-) long sections were cut from the loop for metallographic and chemical analysis. These were cut longitudinally to expose a full half section. Metallographic examination was made in the as-polished and the etched conditions. Wet chemical and electron-beam microprobe analyses were made on selected sections.

In the first half of the boiler, corrosive attack consisted of leaching (selective dissolution and removal) of the more soluble alloy elements (i.e., manganese, chromium, nickel, iron, and cobalt, in the approximate order of their solubility in mercury). The

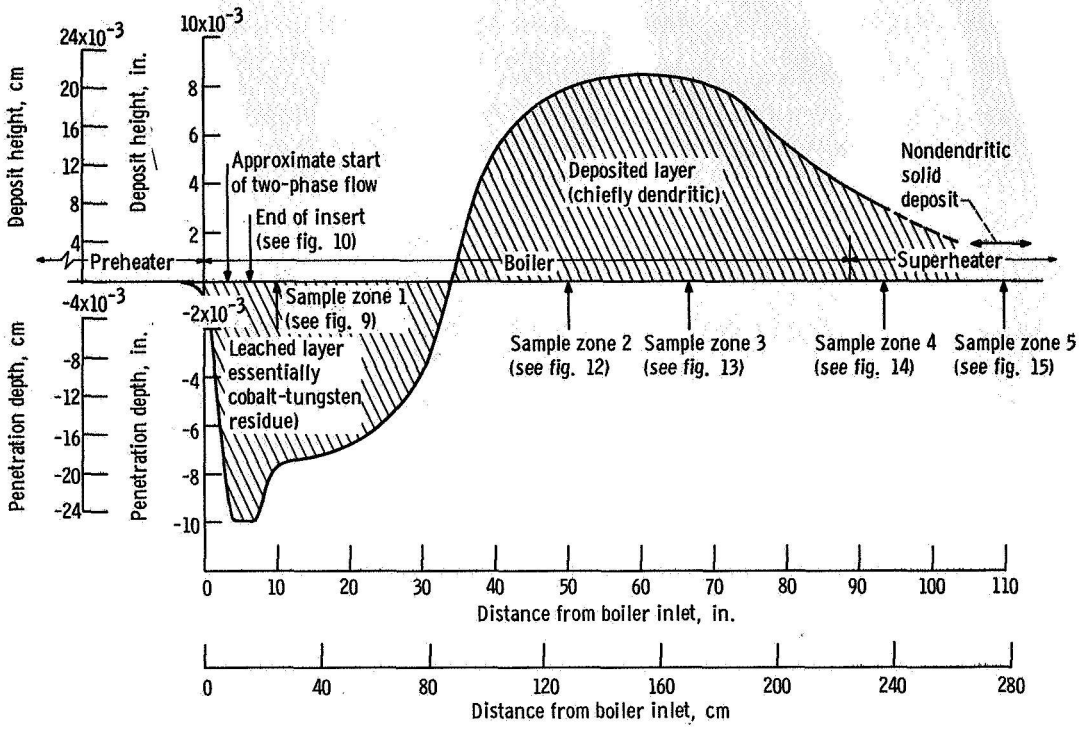

Figure 8. - Variation of maximum penetration depth and maximum deposit height along boiler-superheater.

maximum depth of attack, about 10 mils (2.5×10^{-2} cm), occurred in the boiler insert zone where the peak liquid temperature existed.

No corrosive attack occurred in the second half of the boiler or in the superheater. Instead, the tube surface in these locations was covered with an adherent deposit of material that had been leached from the attacked zones. The depletion-deposition curve in figure 8 is based on the maximum depletion depth or deposit height found in each of a number of representative specimens taken from the loop. The curve in figure 8 is a faired plot that envelops the depletion-deposition pattern.

Typical views of the depletion and deposition zones in the loop are presented and discussed in the following sections.

Corrosive Attack in Boiler

The maximum depth of leaching attack, 0.010 inch (0.025 cm), occurred between 4 and 8 inches (10 and 20 cm) from the boiler inlet near the end of the insert zone. As shown in figure 8, the depletion depth increased sharply in the boiler insert zone. The type and severity of the corrosive attack are illustrated by the photomicrographs shown in figure 9. The leached layer (fig. 9(b)) is barely visible as a dull gray layer on top of

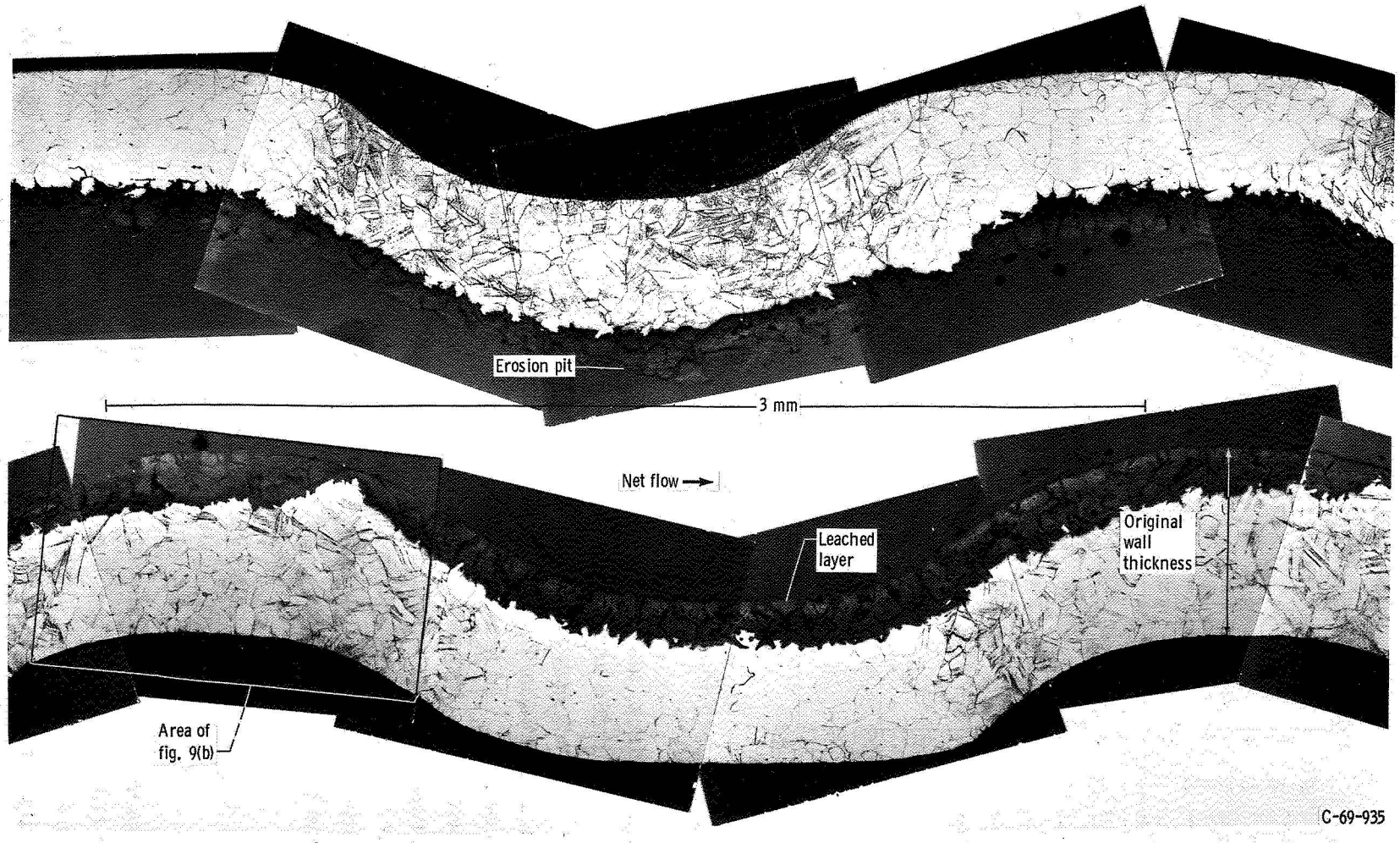

(a) Photomontage showing corrosive attack along upper and lower wall of boiler.

Figure 9. - Section of boiler wall showing typical corrosive attack (sample zone 1 indicated in fig. 8).

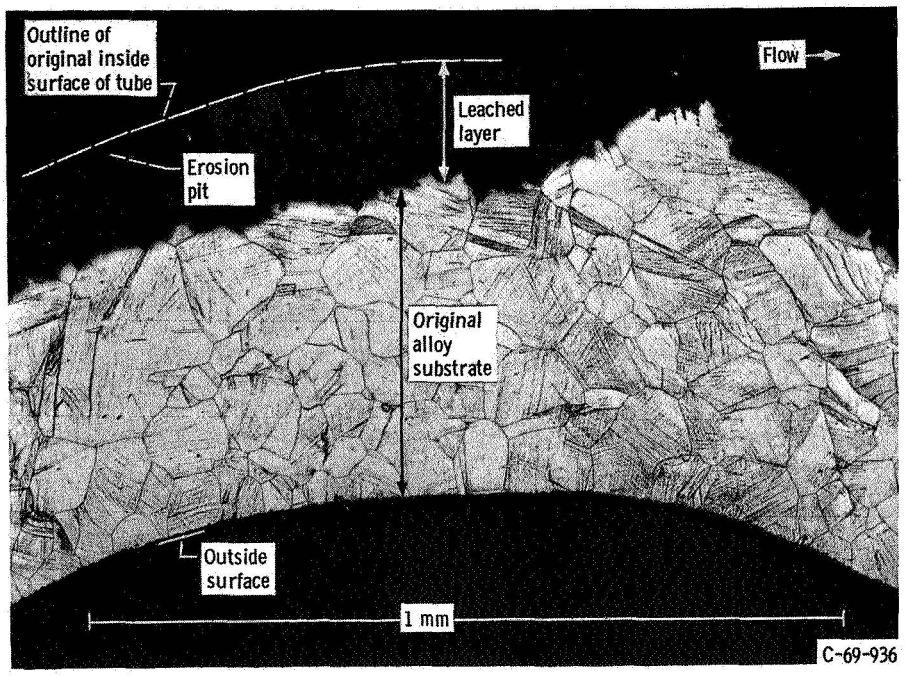

(b) Detailed view of leached layer in boiler wall.

Figure 9. - Concluded.

TABLE I. - COMPOSITION OF CORRODED LAYER AND DEPOSITS IN MERCURY LOOP[a]

Alloy elements (major constituents in order of abundance)	Nominal composition of cobalt alloy HS-25	Boiler-superheater sample zones					Vapor throttle deposits	
		1	2	3		4	5	Type A	Type B
		Reference figures showing location and structure						
		8 and 9	8 and 12	8 and 13		8 and 14	8 and 15	16(b) and (c)	
		Leached layer	Dendritic deposit	Two-phase deposit		Granular deposit	Dense deposit	Sublayer	Overlayer
				Core	Coating				
Cobalt	50 to 52	26 to 40	95 to 99	97.8	83.3	33 to 43	21 to 36	<0.01	0.8
Chromium	19 to 21	1.2 to 1.9	1 to 2	1.3	14.6	27 to 31	30 to 36	5.3	97.5
Tungsten	14 to 16	63 to 39	1 to 2	<0.4	0.4	3.2 to 4.8	7.5 to 12.5	~0.05	0.1
Nickel	9 to 11	0.2 to 0.3	1 to 1.4	<0.02	3.6	18 to 26	12.5 to 21	77.5	1.0
Iron	1 to 3	0.4 to 0.5	~3.9	0.2	0.3	~0.1	0.3 to 0.3	0.2	~0.01
Manganese	1 to 2	[b]<0.1	[b]<0.1	-----	----	---------	----------	17.2	~1

[a]Weight percent obtained by electron-beam microprobe analysis unless otherwise noted.

[b]Weight percent obtained by wet-chemical analysis.

the jagged-appearing interface with the alloy substrate. This layer contains numerous fissures and cracks and consists almost entirely of an insoluble residue.

Results of an electron-beam microprobe analysis are given in table I, which shows that the elemental composition of the leached layer is predominantly cobalt (Co) and tungsten (W). An X-ray diffraction pattern indicated Co_3W and a complex metal carbide of the structure M_6C as major constituents of this layer. Although the layer was fractured in many places, the fractures did not result in significant removal of leached material from the remaining wall. However, a few places showed evidence of slight erosion, spalling, or cracking.

The depth of attack increased sharply from the boiler entrance to a point about 3 inches (8 cm) beyond that at which two-phase flow began (fig. 8) and the liquid temperature peaked. The maximum depth of attack remained approximately 0.010 inch (2.5×10^{-2} cm) for an additional distance of about 3 inches (8 cm) and, beyond this a gradual decrease in attack depth occurred. Where the attack stopped, a dendritic deposit buildup began.

As mentioned previously, the bulk liquid stream flowed more or less uniformly in the helical grooves throughout the boiler. However, the liquid stream was not sharply defined but, in general, tended to spread over the boiler surface. Both the X-ray and metallographic evidence indicated that liquid coverage was fairly uniform because of spreading (by wetting) and agitation. As evident from figure 9(a), the bottom and the top of the boiler tube were nearly equally attacked, and the attack was not confined solely to the deepest portion of the groove channel.

The cylindrical insert in the boiler inlet (see fig. 10) was neither attacked as heavily nor attacked in the same manner as the boiler wall. As mentioned in the section Two-Phase Flow Conditions, the inception of two-phase flow began within the insert zone. Only a small amount of leaching attack was seen on the insert surface. Figure 11 gives evidence that the original tool marks on the insert were generally intact, which suggests that centrifugal forces and a vapor blanket separated the liquid phase from the insert sur-

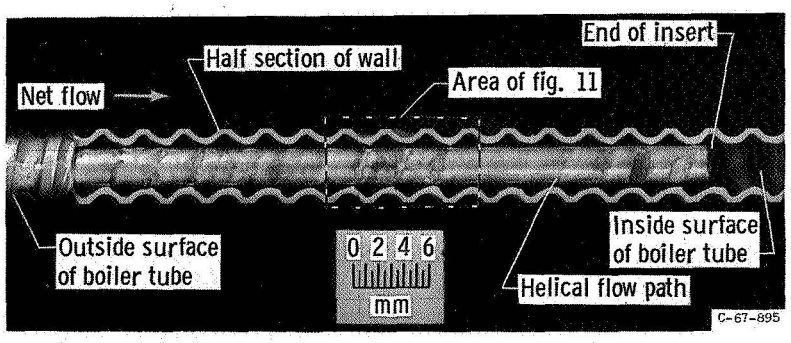

Figure 10. - Cutaway view of boiler inlet showing cylindrical insert and attack after 1147 hours.

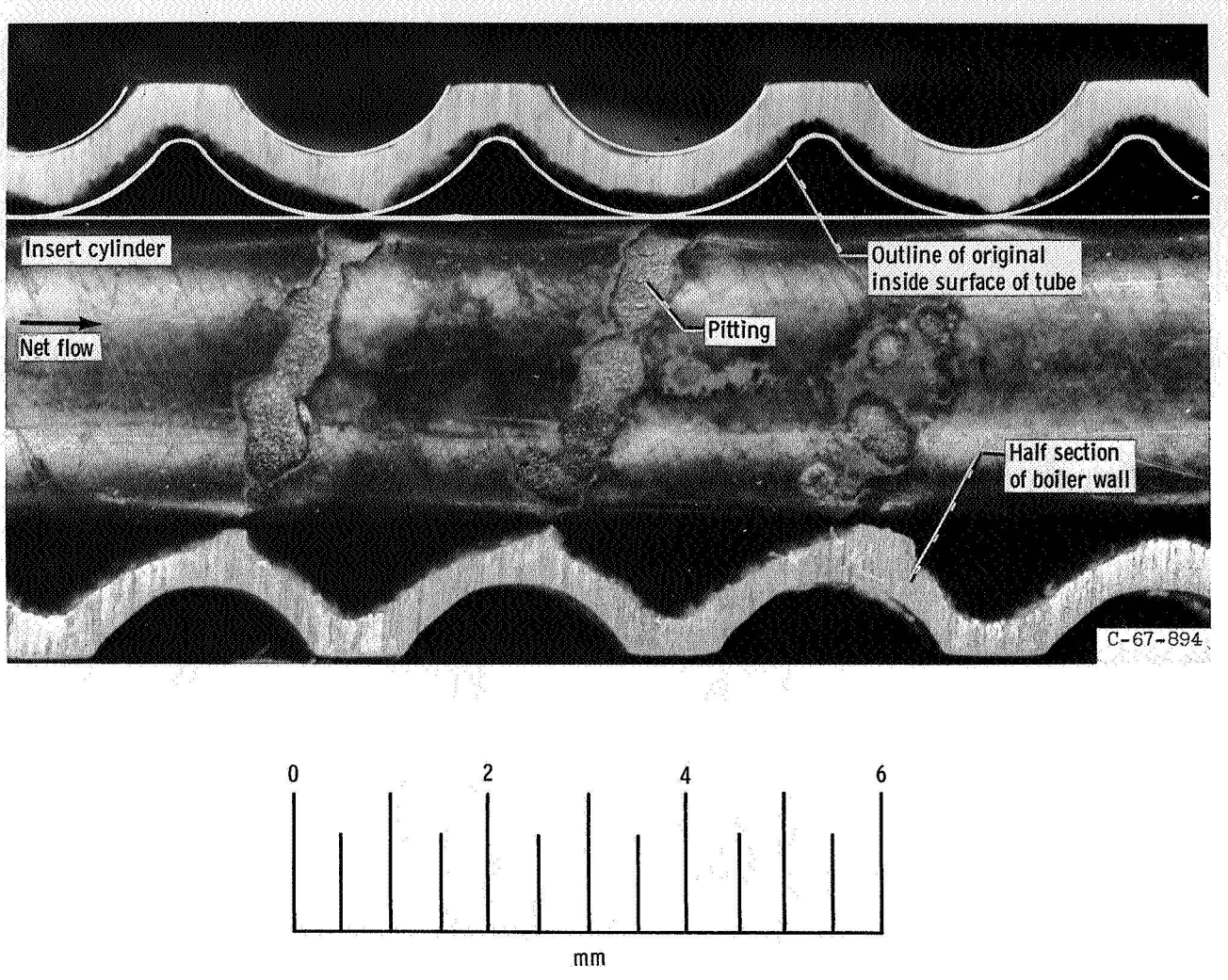

Figure 11. - Detailed view of portion of boiler insert.

face (especially the downstream half where two-phase flow definitely existed).

Irregular pitted grooves occurred on the surface of the insert (see figs. 10 and 11). The broken helical pattern of the pitted grooves corresponded exactly to the helical pattern of the boiler wall; that is, the pitting occurred near the line of contact between the insert and the boiler wall.

Boiler-Superheater Deposits

Approximately halfway into the boiler, the wall depletion depth became nil, and a deposited layer of corrosion products appeared. As indicated in figure 8, the height of

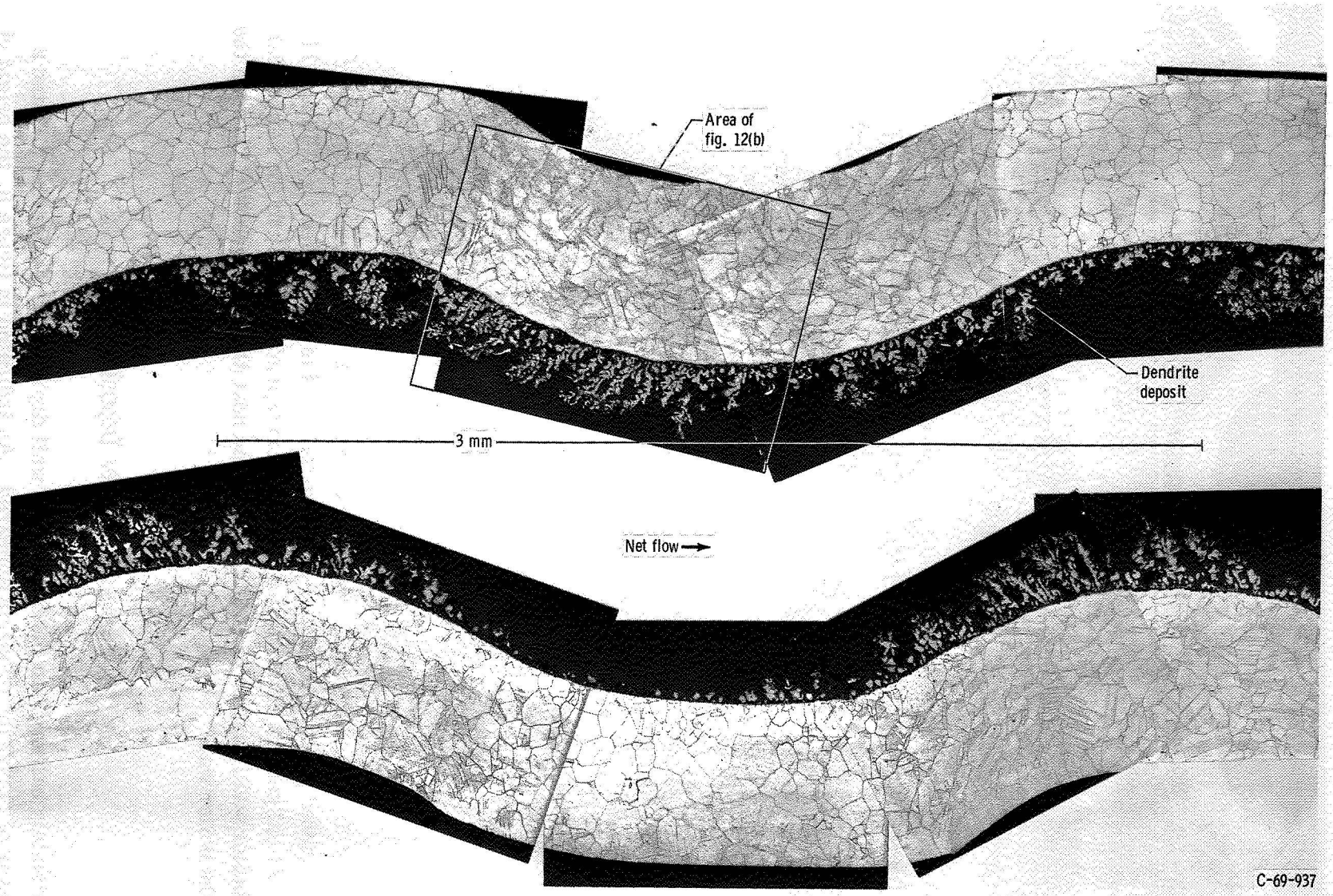

(a) Photomontage showing dendritic deposit along boiler upper and lower wall.

Figure 12. - Section of boiler wall showing typical dendritic deposit (from sample zone 2 indicated in fig. 8).

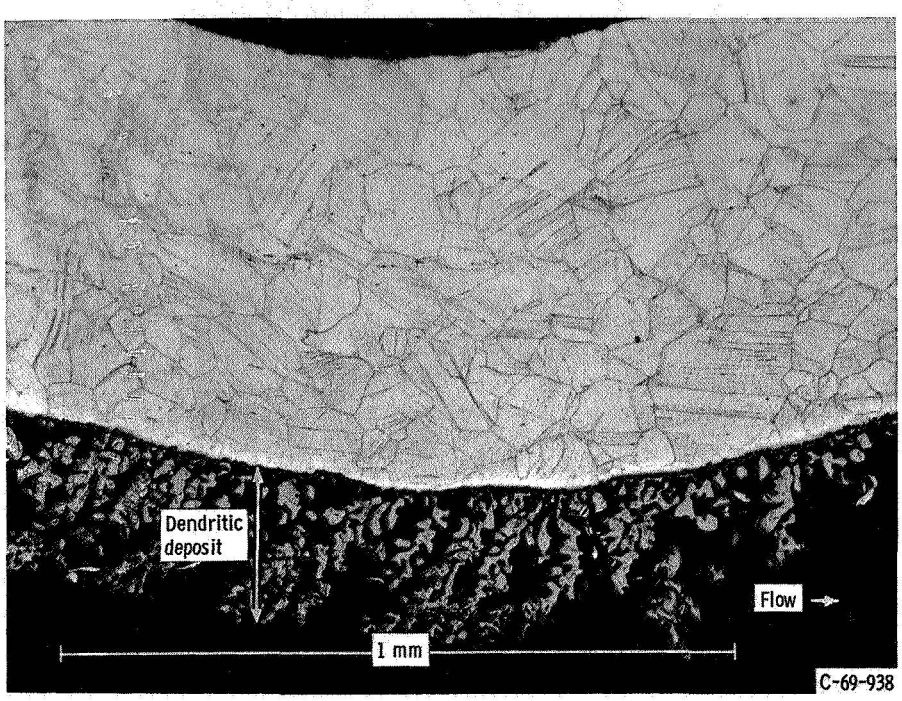

(b) Detailed view of typical dendritic deposit in boiler (from sample zone 2 indicated in fig. 8).

Figure 12. - Concluded.

the layer increased to a maximum of approximately 9 mils (2.0×10^{-2} cm) in the latter half of the boiler. The appearance and apparent nature of the deposit changed with its location along the boiler. An apparent connection existed between the deposit height and the thickness (depth) of the liquid stream at various points along the boiler.

Results of an electron-beam microprobe analysis of deposits removed from the boiler wall at sample zone 2 are given in table I. In this zone, the deposit is cobalt rich. A typical dendritic deposit of the type found in sample zone 2 is shown in figure 12 (also see fig. 8 for location of sample zone). Farther downstream in the boiler (sample zone 3), the deposits showed small amounts of a second phase, which coated the outside of the original dendrites (see fig. 13). Results of electron-beam microprobe analyses made of the two-phase dendrites found in this zone (figs. 8 and 13) are given in table I. The coating on this deposit is also cobalt rich, but it has a considerably greater chromium content than the deposit in zone 2.

At the beginning of the superheater (sample zone 4), another change in the deposits was noted. In this zone, they were compact and granular (see figs. 8 and 14), apparently the result of epitaxial growth (structure and orientation influenced by substrate). An electron-beam microprobe analysis of sample zone 4 is given in table I. The analysis indicated a substantial increase in chromium and nickel content and a corresponding decrease in cobalt content in the deposits within sample zone 4.

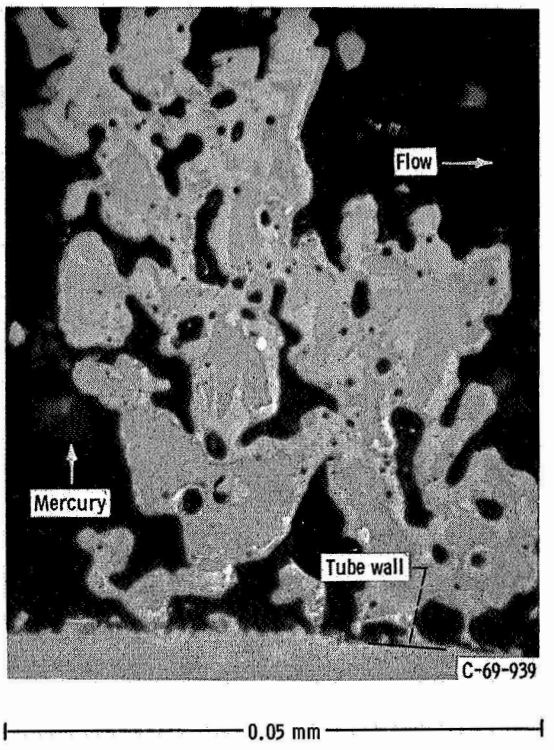

Figure 13. - Detailed view of dendritic deposit (from sample zone 3 indicated in fig. 8) showing variation in composition.

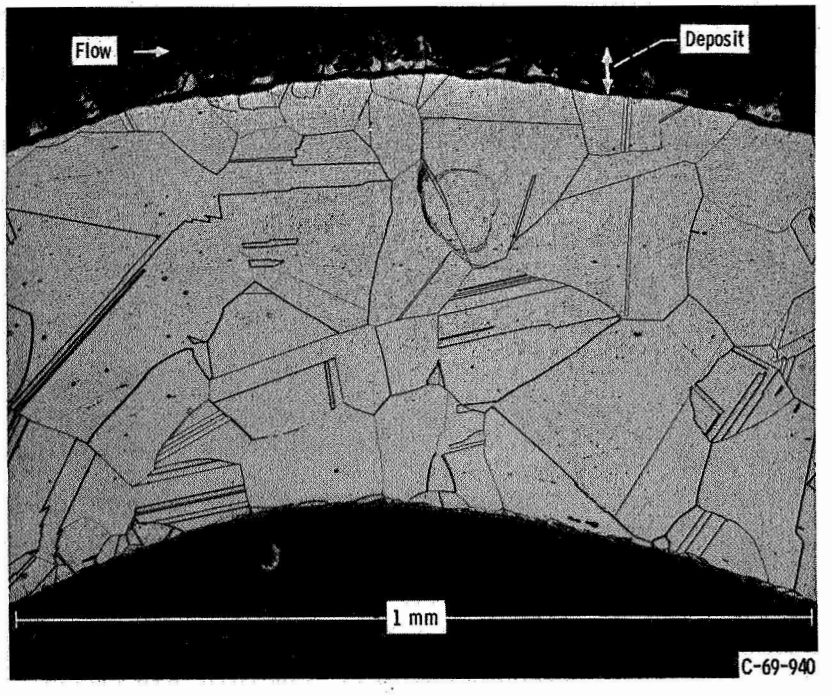

Figure 14. - Typical deposits in first half of superheater (from sample zone 4 indicated in fig. 8).

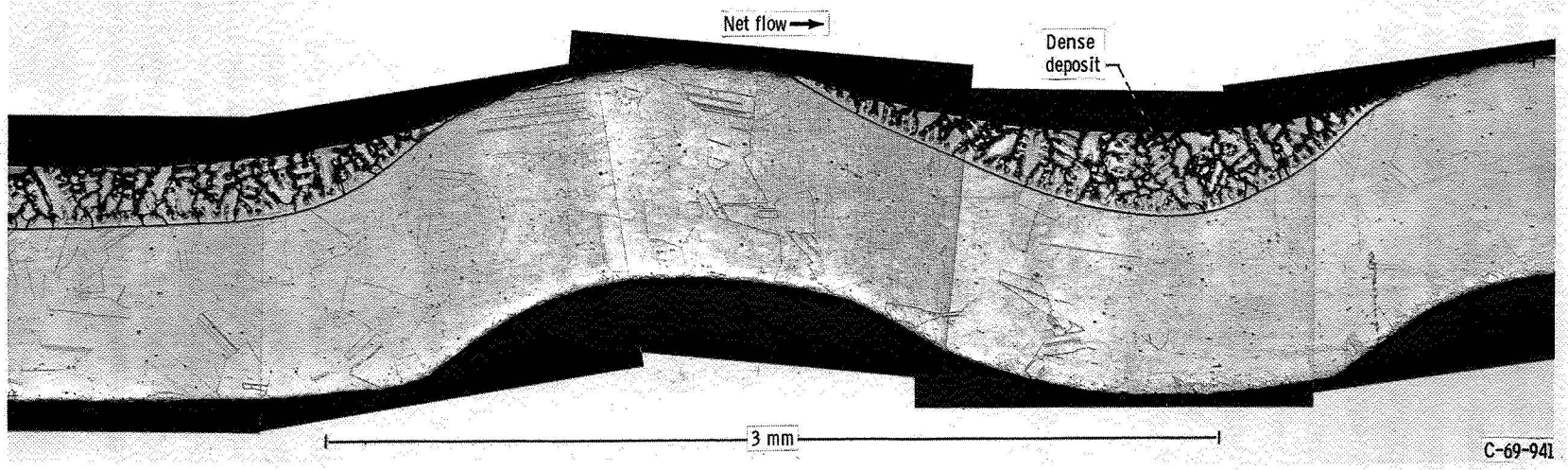

Figure 15. - Typical deposits in last half of superheater (from sample zone 5 indicated in fig. 8).

In the latter half of the superheater (sample zone 5), the deposits were located solely in the helical grooves, where they formed a solid deposit with an appearance suggesting a new solidified alloy with epitaxial growth (see figs. 8 and 15). Close examination revealed no voids in this structure; the surface of this deposit appeared as smooth as the original tube wall. The deposit was compact, coherent, and filled the grooves smoothly to varying depths. The depth varied from nil to a maximum of about 10 mils (2.5×10^{-2} cm) and then back to nil within a distance of about 1 foot (30 cm). No further deposits were present within the last few inches of the superheater exit.

The analytical results given in table I show that the cobalt and iron content of the deposits diminished while the chromium and nickel content increased in the downstream direction from sample zone 2 to 5.

Vapor Throttle and Condenser Deposits

The inlet channel of the vapor throttle was free of deposit buildup. However, a copious accumulation of deposits was present downstream of the throttling orifice. These deposits collected on the conical plug and within the expansion chamber surrounding the inlet tube (see table I and fig. 16). Two different deposits were found in the throttle: deposit A, containing a high percentage of manganese, formed first, followed by a chromium-rich deposit, B. The amount of matter that collected in the vapor throttle, especially in the throttle exit channel, was so great that it completely clogged the flow passage. During the last 10 hours of the 1147 hours of test time, the deposits reduced the flow passage to such a degree that it was impossible to maintain normal operating conditions.

The X-ray motion-picture data collected during the test indicated that most of the vapor throttle deposit accumulated during the final 300 to 500 hours of the test. The accumulation of the throttle deposit was first detected by close observation of the throttle valve X-ray silhouette. Deposit A first became evident after the loop had been operating off-design with wet, low-quality vapor passing through the valve during the latter part of the run.

Essentially all the deposition in the condenser occurred near the inlet where the maximum height of the deposit layer was approximately 2 mils (5×10^{-3} cm). The condenser deposit diminished to nil within 1 foot (30 cm) of the inlet. The condenser deposit was composed of a rather fine granular material that was located in the region where X-ray observation and temperature measurements indicated film condensation. Farther downstream, where liquid droplets began to appear, and beyond, no deposits were present.

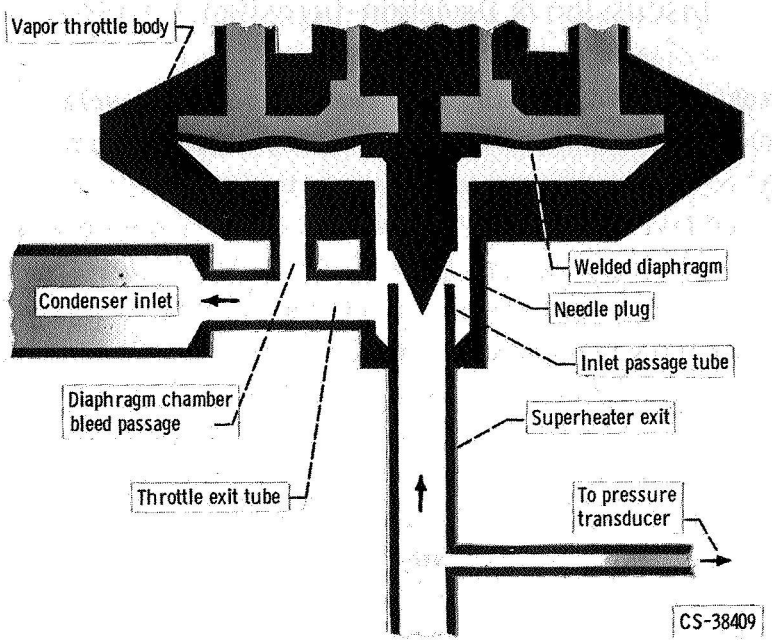

(a) Mercury vapor throttle.

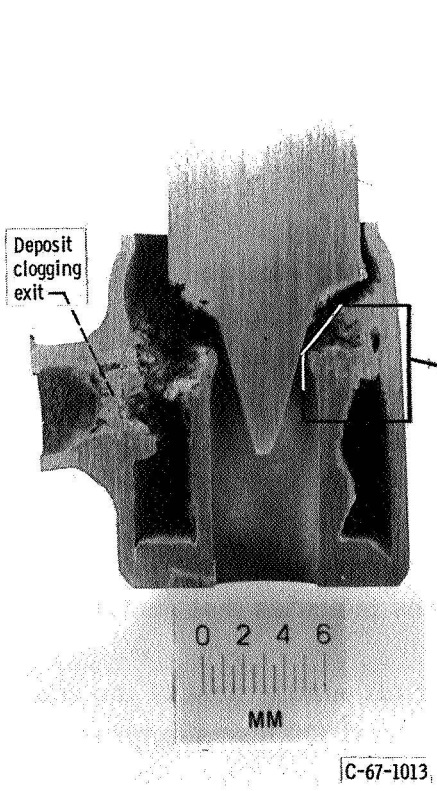

(b) Half-sectional view of vapor throttle orifice showing accumulated corrosion product deposit.

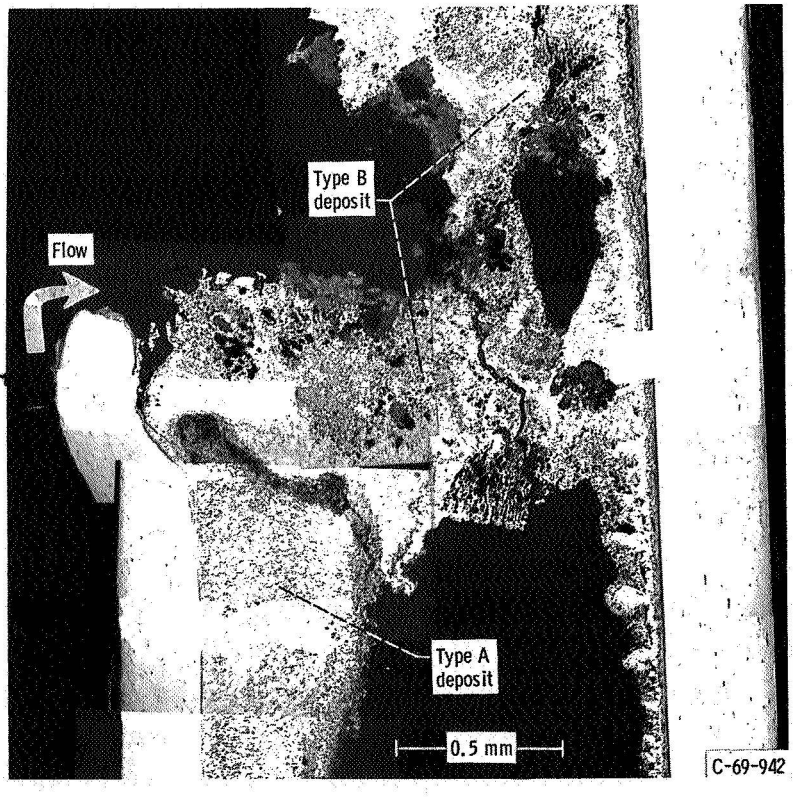

(c) A photomontage of corrosion product accumulation around vapor throttle orifice.

Figure 16. - Sectional views of vapor throttle showing corrosion product accumulations.

Discussion of Depletion-Deposition Results

Wherever attack occurred, it was of the form of selective solution (leaching) of mercury-soluble elements. And, as anticipated, the relative amounts of elements remaining in the leached layer corresponded closely to the relative amounts in the HS-25 reflux capsule leached layer (ref. 4). The leached layer in both cases was a residue consisting predominantly of the material relatively insoluble in mercury.

The depth of attack increased sharply inside the boiler until the maximum depth, 0.010 inch (0.025 cm), was reached in the region where the liquid temperature peaked and two-phase flow began. Beyond this depth, the attack and liquid phase temperature both decreased. The foregoing is in agreement with the expectation that the greatest potential for corrosive attack would exist near the point where the liquid temperature was highest and, hence, the solution capacity was greatest. (Mercury solubility of the alloy elements increases exponentially with temperature.) The deposition began where leaching attack ended, about 35 inches (90 cm) from the boiler entrance (see fig. 8). At this point, the liquid mercury was undoubtedly saturated. Downstream of this point, further vaporization of the mercury caused supersaturation and precipitation of excess solutes as dendritic deposits.

As expected, because of its high solubility in mercury and its low relative abundance in the alloy, the presence of manganese in the deposits increased toward the superheater exit. Because of the very low solubility of tungsten in mercury, the increase in the percent of tungsten in the deposits from sample zones 2 to 5 was unexpected (see table I). This increase might have been the result of its entrainment and deposition in fine particulate form. Tungsten-rich particles were evidently eroded from the leached layer upstream. Particles of the Co_3W residue characteristic of the leached layer were found embedded at various places in the dendritic deposit. Thus, the transport of tungsten is believed to have occurred because of erosive processes acting on the leached layer, instead of normal solution processes.

The unusally compact deposits (see fig. 15) in the last half of the superheater probably formed from a concentrated liquid amalgam. This liquid amalgam probably entered the superheater as helical streamlets that were prominent during off-design intervals. In any case, the location of the deposits solely in the grooves indicates that centrifugal forces influenced the site of their formation.

Deposit buildup in the vapor throttle was either slow or nil during most of the run. The bulk of these deposits was apparently formed during the last 300 hours (approx) of the run when the frequency of off-design intervals began to increase. The material was probably brought in by solute-laden liquid sprays that entered the throttle during these off-design intervals. The segregation of the manganese-rich and chromium-rich deposits (A and B in fig. 16(c)) attests to a rather complicated mass transfer process.

This process may have involved solution of material previously precipitated upstream and its deposition in the throttle.

Region of Maximum Penetration in Boiler

An attempt was made to interpret the loop results in terms of the corrosion mechanisms and rate-controlling factors that prevailed in the region of maximum penetrative attack. In the discussion that follows, maximum depth of attack or penetration is adopted as the prime measure of corrosion to facilitate comparison with the corrosion in mercury reflux capsules (ref. 4).

Plotted in figure 17 are the maximum penetrations observed in this high-velocity loop and in a previous NASA Lewis Research Center loop of HS-25 run for 400 hours (described in appendix B) as well as data for HS-25 reflux capsules run at 1100° F (839 K) (ref. 4) and two other HS-25 loops (refs. 5 and 6) with liquid velocities in the same range as the capsules.

Comparison of these data suggests that velocity has an effect on the corrosion of HS-25 by liquid mercury. For example, in figure 17 the maximum penetrations for the 400- and 1147-hour NASA loops fall far outside the 4-sigma standard deviation envelope of the capsule plot. By contrast, the penetration depths of the low-velocity loops of references 5 and 6 fall well within the standard deviation envelope. This envelope consists

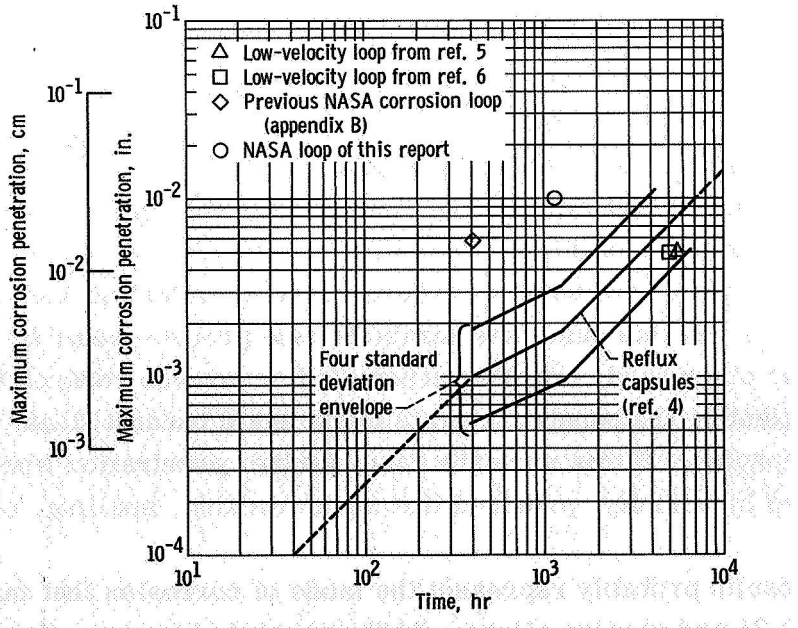

Figure 17. - Comparison of corrosion loop data with reflux capsule results obtained at 1100° F (868 K).

of a total span of four standard deviations in figure 17; that is, two sigma above and two sigma below the mean represented by the capsule data.

Corrosion mechanisms. - The corrosion mechanisms operating in the loop are believed to be the same as those previously observed in the HS-25 mercury reflux capsules (ref. 4). Because there are not enough HS-25 loop data, corrosion rates and the effect of velocity cannot be determined directly. However, some significant inferences concerning rates can be made.

Reference 4 explained that in reflux capsules three different rate stages were involved in the corrosion of HS-25 by mercury. In the first stage, penetration increased linearly with time; in the second stage, penetration increased in proportion to the square root of time; and in the third stage, penetration again increased linearly with time. The corrosion mechanisms associated with each of these stages are discussed in appendix C.

Based on an analysis of the leached layer, we believe that only the first two of these stages prevailed during the 1147-hour loop run (and also in the 400-hr loop). We further believe that the effect of velocity prevailed only during the relatively brief initial linear stage of the corrosion process. Although the velocity-dependent stage is believed to have lasted less than 15 hours, it had a pronounced effect on the depth of attack, as seen in figure 17. A discussion of the rate change and velocity effect interpretations of the loop data is presented in appendix D.

Nature of corrosion layer. - A second linear rate process might have eventually occurred in the loop. We believe this is unlikely because the cracks in the leached layer of the loop differed from those of the capsules of reference 4 (see appendix C). The thickness of the leached layer beyond the root of the cracks in the loop remained significantly greater than that in the capsules. There was no indication that crack propagation toward the substrate in the leached layer of the loop would result in a second linear stage. After 1147 hours, the leached layer of the loop was essentially intact. In addition, the leached layer of the loop was considerably thicker, even after 1147 hours, than the thickness attained in the capsules after 5000 hours.

The leached layer in the loop might have remained intact beyond several thousand hours of operation. In this case, the parabolic rate process would be expected to continue. If, on the other hand, cracking penetrated or erosion reduced the leached layer thickness sufficiently, the penetration rate might again become linear as it did in the HS-25 reflux capsules. If this were the case, further penetration would once more be strongly affected by velocity, provided that such cracking, spalling, or erosion effects continued.

The loop results probably represent the mode of corrosion that may be expected in general with HS-25 and similar alloys. At the present, however, there is insufficient information regarding the differences observed in the inception of the leached layer cracking or spalling in capsules and loops. Undoubtedly, the leached layer in the loop

was subject to different thermal-mechanical stresses than was the layer in the capsules. The differences in stress effects could have delayed or precluded the onset of the second linear stage in the corrosion process in the loop. The results are probably highly dependent on the alloy and possibly on heat treatment and fabrication history. (Neither the loop nor the reflux capsules were heat treated after fabrication and welding.)

Further Considerations

Factors influencing penetration maximums. - If the mercury entering the boiler can be assumed essentially pure, the penetration results can be viewed as maximums under the flow and temperature conditions that prevail. Conversely, if other than virgin mercury enters the boiler, the severity of the penetration would not necessarily represent a maximum. Considering the precautions taken and the loop conditions that prevailed, the latter is unlikely. In any case, the greatest potential for corrosion existed in the boiler inlet zone where the peak liquid temperature existed.

Another factor to be considered in two-phase flow involving nucleate boiling is the continuity of the liquid phase. X-ray observations revealed no discernible breaks in the bulk liquid streamlet in the region of maximum attack. It seems fairly certain that at least the mercury film coverage was constant and unbroken in this region. In this case, the measured penetrations are true maximums in terms of the constant and essentially uniform exposure to liquid mercury.

Pitting and erosion. - The irregular pitting on the boiler insert (see figs. 10 and 11) may be attributed to cavitation damage. The configuration of the insert zone and the presence of nucleation (boiling) were conducive to pseudocavitation. Vapor bubbles were probably entrained in the flow stream and forced against the insert near the line of contact between the boiler tube groove and insert. A slight difference in temperature of the insert surface relative to the vapor bubble could lead to bubble collapse and thereby induce cavitation. The similarity in appearance between the pitting attack observed here and that observed in mercury cavitation damage studies (ref. 10) lend support to the contention mentioned previously.

Evidence exists of erosion of the leached layer in the insert zone opposite the pits in the insert (fig. 11). The effects of erosion are also discernible at other points in the boiler leached layer (fig. 9). Erosion is invariably evident in those parts of the leached layer surface that were exposed to the higher liquid stream velocities.

Corrosion-product transport. - A quantitative evaluation of mass transfer in the loop was precluded because of the complex nature of the processes involved. It was recognized that solution and precipitation were not necessarily the sole contributors to the mass transfer processes. Possibly, some material was transported as undissolved entrainment or in colloidal suspension. For example, a suspension of chromium might

have been carried by the essentially dry vapor through the superheater and into the vapor throttle. Entrainment of particles of Co_3W in the mercury streamlet might account for the somewhat unusual distribution of tungsten in the deposits mentioned previously (see Discussion of Depletion-Deposition Results). The entrainment and suspension were probably caused by the erosive processes in the leached layer and deposits.

There are some indications that the deposit pattern in the boiler, superheater, and vapor throttle may have been formed in consecutive stages. These stages were not necessarily generally connected with the off-design conditions mentioned previously. For example, the source of the chromium-rich deposits in the vapor throttle may have been the precipitates that formed initially in the boiler-superheater. Thus, deposit buildup in the throttle might have been a mass transfer stage that occurred after leaching and deposition in the boiler-superheater had reached a certain level.

SUMMARY OF RESULTS

A two-phase, forced-convection mercury loop constructed of the cobalt-base alloy HS-25 (L-605) was operated for 1147 hours with a liquid velocity of about 8 feet per second (240 cm/sec). The peak temperature in the boiler was 1075° F (858 K). The maximum vapor temperature in the superheater was 1300° F (977 K). Post-test examination of the loop revealed severe corrosion near the boiler inlet where two-phase flow began and the liquid temperature reached its peak value. A maximum penetration depth of 10 mils (2.5×10^{-2} cm) was observed in this region. This depth was significantly greater than would be expected based on a direct comparison with the results of reflux capsule or lower velocity mercury loop tests of the alloy. This penetration indicates that liquid velocity was an important corrosion parameter, at least in the early stages of loop operation.

The corrosion in the loop was similar in many respects to that found in HS-25 (L-605) reflux capsules in which crucial corrosion mechanisms could be identified. This identification made it possible to reach tentative conclusions regarding the rate controlling processes that occurred in the loop.

Lewis Research Center,
National Aeronautics and Space Administration,
Cleveland, Ohio, March 10, 1969,
120-27-02-18-22.

APPENDIX A

SURFACE DECONTAMINATION AND CONDITIONING PROCEDURES

Chemical Cleaning

The chemical cleaning of the loop and its components was done in the following sequence:

(1) Ultrasonic liquid or vapor degreasing

(2) Ultrasonic alkaline detergent cleaning followed by distilled water rinsing

(3) Warm etching with 5 percent hydrochloric acid (HCl) and 5 percent sulfuric acid (H_2SO_4) (small parts dipped for 60 min and the acid solution was pumped through long tubular parts for 60 min)

(4) Passivation etching with 13 percent nitric acid (HNO_3) and 2 percent hydrofluoric acid (HF) solution (same procedure used as in step 3)

(5) Final distilled water rinsing until a neutrality of about pH 7 was indicated followed by a water-pumped-argon drying-out and backfilling

All components were sealed in plastic bags or capped while awaiting further fabrication or integration into the loop. All welds were made by an inert-gas-enveloped electric arc using HS-25 wire filler. A flowing argon purge was maintained within the loop during final assembly.

Loop Thermal Conditioning

In the assembled loop, after cleaning, evacuation, and mercury filling, wetting was induced in the pump cell and boiler by heating to a temperature of about 1100° F (868 K). Heating was done initially under zero flow conditions. When the temperature reached approximately 1100° F (868 K), further heating was done with mercury flowing at a rate of about 100 pounds per hour (0.013 kg/sec).

Evidence of mercury wetting by this thermal-conditioning method was most noticeable in the electrodynamic pump. As explained in reference 11, the developed pressure in the pump was directly related to the degree of wetting.

The existence of adequate wetting in the boiler could be inferred from the character of the mercury flow pattern and from the ease in attaining stable boiling. The flow pattern observations and attainment of stable boiling indicated that about 2 hours were sufficient to secure adequate wetting in the boiler at temperatures between 1050° and 1100° F (839 and 868 K).

After initial wetting had been accomplished, the loop could be shut down, cooled to room temperature, and then restored to preshutdown conditions within 5 to 10 minutes. This completed the evidence indicating that prior to the shutdown relatively complete wetting existed. Also apparent was the fact that only slight dewetting occurred during shutdown in the absence of air leak-in. Previous experience indicated that dewetting invariably occurred when the wetted interface was exposed to air.

APPENDIX B

DESCRIPTION OF PRIOR NASA LEWIS RESEARCH CENTER MERCURY LOOP

A prototype of the 1147-hour mercury loop described in this report was operated for 400 hours with a peak liquid temperature of approximately 1100° F (868 K). As in the loop of this report, the maximum penetration occurred in the region of the temperature peak and about 3 inches (8 cm) downstream of the locus of two-phase inception.

The 400-hour loop was fabricated from the same HS-25 tubing as the 1147-hour loop. The 400-hour loop boiler consisted of tubing that was swaged with a helical groove identical to the one described previously in the APPARATUS section. However, the 400-hour loop did not have an insert. Therefore, in the all-liquid portion of the boiler inlet, the axial-flow velocity was about 1 foot per second (30 cm/sec). Downstream of the locus of two-phase inception, the liquid phase tended to follow the helical grooves and had a tangential velocity component of about 3 feet per second (90 cm/sec). (The mercury flow pattern was observed by X-ray as in the 1147-hr loop.)

The maximum depth of penetration in the 400-hour loop was 5.8 mils (15×10^{-3} cm). The appearance and composition of the leached layer corresponded closely with that in the 1147-hour loop. Detailed examination of mass transfer effects was not undertaken with the 400-hour loop (outside the region of maximum corrosion).

APPENDIX C

CORROSION RATE-CONTROLLING PROCESSES

The following discussion is based on the three-stage corrosion of HS-25 described in reference 4. The three stages are briefly termed linear I, parabolic, and linear II.

Linear I: Diffusion in Boundary Layer Controlling (Linear Time Rate)

The basic mode of corrosion in the loop and capsules was simple solution of the boiler-wall alloy constituents. At first, the rate of transfer of dissolved material into the bulk liquid stream depended on diffusion through the liquid boundary layer. This diffusion is the rate-controlling process in the case of solids that are readily soluble in mercury (ref. 2), as in the case of most of the constituents of HS-25. In accordance with this concept, the depth of penetration should vary linearly with time (ref. 12):

$$p \propto D_b t \tag{C1}$$

where p is the (maximum) depth of penetration, D_b is the boundary layer diffusion coefficient, and t is time.

Parabolic: Diffusion in Leached Layer Controlling (Parabolic Time Rate)

After an interval of time, the leached layer becomes depleted of readily soluble species. This process, in the case of the alloy HS-25, results in the creation of a porous, sponge-like zone composed of a relatively insoluble residue material. This porous matrix becomes saturated with liquid that provides a medium for solute mass transport from the substrate to the liquid stream. Eventually, as explained in reference 4, diffusion through the quiescent liquid in the porous layer becomes the limiting or rate-controlling process. This diffusion limitation appears to occur after the leached layer attains a certain critical thickness, approximately 1 mil (2.5×10^{-3} cm) in the case of the HS-25 capsule tests. The time-penetration relation for mass transfer through the liquid-filled leached layer gradually becomes parabolic as the layer thickness increases:

$$p \propto (D_l t)^{1/2} \tag{C2}$$

where D_l is the coefficient for diffusion through the liquid-filled, porous (leached)

layer. The time dependence is the same as that derived in reference 12 when a moving boundary exists. In the present case, the moving boundary is the interface between the unleached solid substrate and the leached layer.

Linear II: Resumption of Diffusion in Boundary Layer Controlling (Linear Time Rate)

In the HS-25 reflux capsules of reference 4, the linear time rate resumed after the leached layer thickness exceeded a certain depth. Cracking and spalling of the leached layer occurred as the depth increased. This cracking and spalling ultimately exposed or tended to expose the unleached solid substrate. The linear rate resumed because the roots of the cracks penetrated to within less than the 1-mil (2.5×10^{-3}-cm) critical thickness that marked the inception of the second stage. Furthermore, the crack roots continually propagated toward the substrate, thereby ensuring the continuance of the second linear rate.

APPENDIX D

CORROSION RATE CHANGE AND VELOCITY EFFECT

In the 1147-hour loop of this report, the time-dependence probably became parabolic and, hence, independent of velocity when a "critical" leached layer thickness had been reached. Prior to this event, the rate was probably linear with time. The rate processes and rate change from linear to parabolic can be inferred from the capsule study of reference 4 (as abstracted in appendix C). Note that the term critical thickness as used herein denotes an approximation. As stated in reference 4, the change in time dependence was continuous and should not be construed as altering abruptly when the critical thickness was reached.

The critical leached layer thickness for HS-25 reflux capsules was approximately 1 mil (2.5×10^{-3} cm) (ref. 4). Herein, it is deemed reasonable to suppose that corrosion rate changeover also occurred in the loop when the leached layer thickness became 1 mil (2.5×10^{-3} cm).

Velocity Effect in Boundary Layer Diffusion

According to reference 2, convective diffusion in the boundary layer is influenced by the linear velocity of the bulk liquid. Evidence of this velocity effect on corrosion processes has been cited by previous investigators (e.g., see refs. 8 and 9). In the previously cited references and in references 2 and 3, corrosive penetration is shown to vary with velocity under certain conditions. For example, let the penetration rate p by corrosive attack be taken as being directly proportional to the mass transfer rate across the liquid boundary layer at the wall w. Therefore,

$$p \propto \int_0^t w \, dt \tag{D1}$$

Note that the rate w will, in general, vary with time.

According to reference 2, w and therefore p will vary exponentially with liquid velocity if all other conditions are held constant:

$$p \propto v^e \tag{D2}$$

where p is maximum depth of penetration, v is velocity, and e is a constant. The author of reference 2 suggested that e should be nearly 1 or perhaps about 0.8. This

value is based on empirical heat-transfer relations (ref. 13) and is widely quoted.

Two restrictions in applying the relation expressed by equation (D2) are (1) the equation applies specifically to fully-developed turbulent flow when an exponent e equal to or greater than approximately 0.8 is used, and (2) the equation applies specifically to cases where a boundary layer exists, and diffusion therein is rate controlling. Accordingly, the velocity dependence of penetration in the loop should have prevailed only during the relatively brief period when the leached layer thickness grew to a critical magnitude of approximately 1 mil (2.5×10^{-3} cm). This period is assumed to be about 12 hours and was found by extending a half-power line from the 1147-hour data point in figure 17 (p. 23) to intercept the 1-mil (2.5×10^{-3}-cm) ordinate. Note that each of the two NASA Lewis Research Center loop points in figure 17 should lie on different lines having slopes of one-half in a logarithmic plot of penetration against time. This is because the velocities and flow channel geometries in these two loops were not the same.

Velocity Effect Interpretation

Certain precautions should be used in handling penetration data obtained with materials subject to the velocity and rate change effects described in the previous section. Particular attention should also be given to the fact that the maximum attack may occur in a region where two-phase flow and nucleation exist. In this latter case, as in the loops reported herein, it is important to know the liquid phase flow patterns and thereby have a better idea of conditions existing in the region of maximum attack.

A complication arises in the case of materials like HS-25 if penetration measurements are made after a penetration rate change has occurred (presumably from linear to parabolic). Interpretation of loop results for velocity effects should then follow the procedure suggested in the next paragraph.

Assume that two high-velocity loops have been operated for the same length of time under identical conditions except for velocities. The penetration depths p_1 and p_2 will be related to the velocities by the expression $p_1/p_2 = (v_1/v_2)^e$ only if the measurements are taken during the interval when boundary layer diffusion is rate controlling. If the rate process is assumed to change from linear to parabolic at the same critical thickness in each loop irrespective of the velocity level, the relation between penetrations and velocities becomes

$$\frac{p_1}{p_2} = \left(\frac{v_1}{v_2}\right)^{e/2} \tag{D3}$$

where p_1 and p_2 are the maximum depths measured after the time dependence of penetration changed from linear to parabolic.

REFERENCES

1. Slone, Henry O.: SNAP-8 Development Status. Space Power Systems Advanced Technology Conference. NASA SP-131, 1966, pp. 147-168.

2. Epstein, Leo F.: Static and Dynamic Corrosion and Mass Transfer in Liquid Metal Systems. Chem. Eng. Prog. Symp. Ser., vol. 53, no. 20, 1957, pp. 67-81.

3. Horsley, G. W.: Mass-Transport and Corrosion of Iron-Based Alloys on Liquid Metals. J. Nucl. Energy, pt. B: Reactor Tech., vol. 1, no. 2, 1959, pp. 84-91.

4. Rosenblum, Louis; Scheuermann, Coulson; Barrett, Charles A.; and Lowdermilk, Warren H.: Mechanism and Kinetics of Corrosion of Selected Iron and Cobalt Alloys in Refluxing Mercury. NASA TN D-4450, 1968.

5. Cooper, David B.: Operation of a Forced Circulation, Haynes Alloy No. 25, Mercury Loop to Study Corrosion Product Separation Techniques. NASA CR-241, 1965.

6. Schulze, R. C.; and Cooper, D. B.: Operation of a Haynes Alloy No. 25 Forced Circulation Loop to Study the Effects of Hydrogen in a Simulated Sunflower System. NASA CR-225, 1965.

7. Cooper, D. B.; and Vargo, E. J.: Operation of a Forced Circulation, Croloy 9 M, Mercury Loop to Study Corrosion Product Separation Techniques. NASA CR-217, 1965.

8. Kimura, L. A.: Corrosion Mechanism Loop-1 Summary Report. Rep. AN-SNAP 67-346, Aerojet-General-NEMO, Jan. 25, 1967.

9. Hopenfeld, J.; and Darley, D.: Dynamic Mass Transfer of Stainless Steel in Sodium Under High-Heat-Flux Conditions. Rep. NAA-SR-12447, Atomics International, July 15, 1967.

10. Young, Stanley G.; and Johnston, James R.: Accelerated Cavitation Damage of Steels and Superalloys in Sodium and Mercury. NASA TN D-3426, 1966.

11. Vary, A.: Electrodynamic Mercury Pump. NASA TN D-2965, 1965.

12. Crank, J.: The Mathematics of Diffusion. Clarendon Press (Oxford), 1956, pp. 43-60.

13. McAdams, William H.: Heat Transmission. Second ed., McGraw-Hill Book Co., Inc., 1942, pp. 166-168.

NASA-Langley, 1969 —— 17 E-4561

NATIONAL AERONAUTICS AND SPACE ADMINISTRATION
WASHINGTON, D. C. 20546

OFFICIAL BUSINESS

FIRST CLASS MAIL

POSTAGE AND FEES PAID
NATIONAL AERONAUTICS AN
SPACE ADMINISTRATION

POSTMASTER: If Undeliverable (Section 158 Postal Manual) Do Not Return

"The aeronautical and space activities of the United States shall be conducted so as to contribute . . . to the expansion of human knowledge of phenomena in the atmosphere and space. The Administration shall provide for the widest practicable and appropriate dissemination of information concerning its activities and the results thereof."

—NATIONAL AERONAUTICS AND SPACE ACT OF 1958

NASA SCIENTIFIC AND TECHNICAL PUBLICATIONS

TECHNICAL REPORTS: Scientific and technical information considered important, complete, and a lasting contribution to existing knowledge.

TECHNICAL NOTES: Information less broad in scope but nevertheless of importance as a contribution to existing knowledge.

TECHNICAL MEMORANDUMS: Information receiving limited distribution because of preliminary data, security classification, or other reasons.

CONTRACTOR REPORTS: Scientific and technical information generated under a NASA contract or grant and considered an important contribution to existing knowledge.

TECHNICAL TRANSLATIONS: Information published in a foreign language considered to merit NASA distribution in English.

SPECIAL PUBLICATIONS: Information derived from or of value to NASA activities. Publications include conference proceedings, monographs, data compilations, handbooks, sourcebooks, and special bibliographies.

TECHNOLOGY UTILIZATION PUBLICATIONS: Information on technology used by NASA that may be of particular interest in commercial and other non-aerospace applications. Publications include Tech Briefs, Technology Utilization Reports and Notes, and Technology Surveys.

Details on the availability of these publications may be obtained from:

SCIENTIFIC AND TECHNICAL INFORMATION DIVISION

NATIONAL AERONAUTICS AND SPACE ADMINISTRATION

Washington, D.C. 20546